Available online at www.sciencedirect.com
ScienceDirect
Journal of Power Sources 159 (2006) 728–733
JOURNAL OF POWER SOURCES
www.elsevier.com/locate/jpowsour

A simple and robust fiber optics system for measuring the lead-acid battery state-of-charge

O.D. Cortázar*, V. Feliu

Escuela Técnica Superior de Ingenieros Industriales,
Universidad de Castilla-La Mancha – Campus Universitario de Ciudad Real, Ciudad Real 13071, Spain

Received 7 January 2005; received in revised form 5 October 2005; accepted 3 November 2005
Available online 6 January 2006

Abstract

A simple, robust and low-cost fiber optics system for monitoring the state-of-charge (SOC) in a lead-acid battery is presented. The device is based on measuring light ray trajectory variations produced by the electrolyte media when its density changes. The changes in the electrolyte refraction index are produced due to changes in density, and the system measures such changes by means of an optical sensor coupled with a fiber optics bundle. SOC is indirectly measured on the base of such optical specific gravity measuring. A set of equations based on a paraxial ray model perform the optical sensor design, describing its behavior for different design parameters thereby allowing for the optimization of signal response. The system is applied to an SLI battery discharge–charge cycle obtaining excellent agreement with direct measuring of electrolyte density and estimation of SOC by integration of current. Simplicity, low cost, robustness and the unnecessary use of any signal processing are the main improvements with respect to previous works.

Keywords: Lead-acid; State-of-charge; Fiber optics monitor

1. Introduction

Determining the state-of-charge (SOC) of lead batteries is an important issue in several fields of engineering applications, mainly those related to deep discharges produced during heavy-duty services. Vehicle propulsion for robotics systems, wheel chairs and submarine devices are typical examples where knowing the SOC is critical in order to optimize energy management and increase battery life. Several devices for the determination of the SOC have been proposed, mainly using electrical measurements of discharging voltage and battery current with different algorithms [1–4]. The application of wire-wound coils [5–8], measuring the change of inductance associated to the chemical reactions on the negative end plate, is an outstanding application in non-invasive type sensors, but this technique requires the use of sophisticated equipment sensitive enough to detect small changes in the coil inductance during battery cycling. On the other hand, several patents associated to the development of optical sensors [9,10] that use buoyancy in order to determine the density of the electrolyte have been recently published, and optical absorption is proposed by Weiss [11] as an effective method. A device based on the measurements of changes in the electrolyte refraction index was proposed by Hancke [12] describing a fiber optics technique for determining the specific gravity of a lead-acid battery electrolyte. The device proposed by Hancke works by monitoring the leakage of light through the walls of a bent fiber optics soaked in the electrolyte. The light leakage is related to the ratio between the electrolyte and fiber refraction indexes allowing the measure of the specific gravity, and thereby determining the SOC. Moreover, the small signal obtained makes the utilization of electronic amplification and filtering necessary. In this work, a simple fiber optics set up is proposed based on the application of a typical industrial fiber optics bundle probe used for UV–VIS reflective fiber optics spectroscopy. By using a visible source of light, and one optical sensor inserted at the tip of the bundle designed by the authors, the system is sensitive enough to avoid any amplification or treatment of the output signal and presents a lineal behavior by choosing an adequate set of construction parameters.

* Corresponding author.
E-mail address: OsvaldoDaniel.Cortazar@uclm.es (O.D. Cortázar).

0378-7753/$ – see front matter © 2005 Elsevier B.V. All rights reserved.
doi:10.1016/j.jpowsour.2005.11.052

2. Optical system description

A fiber optics bundle is a group of fiber optics packed into a tight cylindrical and flexible package. The diameter of each fiber is typically about 10 μm. Depending on how the individual fibers are placed in the package, we can find two main kinds of bundles: coherent and incoherent bundles. The coherent bundle retains the position of every fiber along the total length of the arrangement so that it is possible to transmit an image along the bundle. This kind of bundle is used when the application requires knowing the position of incoming light at the input of the bundle. The incoherent bundle is characterized by disorder so that the fibers do not retain their original positions.

For this application, we use a special kind of coherent bundle denominated T that has a radial distribution of the fibers in two groups: an inner group of fibers in the center and an annular group arranged around the inner group. In this kind of bundle, the fibers go into the package all together up until one arbitrary point where both groups are separated into two different sub-bundles. Each sub-bundle corresponds to a group of fibers (inner or annular) at the end of the original bundle. The separation between the groups allows the two fiber groups to be used for different tasks: one group for injecting light and the other for collecting it by connecting the sub-bundles to a lamp and a photodiode, respectively. Fig. 1 shows a conceptual layout used in this work where Fig. 1(a) is a tungsten lamp Ocean Optics mod. LS-1 [13], Fig. 1(b) is a T bundle Ocean Optics mod. T300 [13], Fig. 1(c) is the electrolyte of the battery cell interrogated and Fig. 1(d) is a photodiode Thorlabs mod. DET210 [14].

The end of the bundle soaked in the electrolyte interrogates the electrolyte's refraction index by using an optical sensor inserted at the tip. Fig. 2 shows the design of such a sensor that works as an optical transducer by measuring the specific gravity detecting small changes in the refractive index. The sensor is basically composed by a Teflon cylindrical chamber (Fig. 2(a)) divided in two parts by a lens of BK7 glass (Fig. 2(b)).

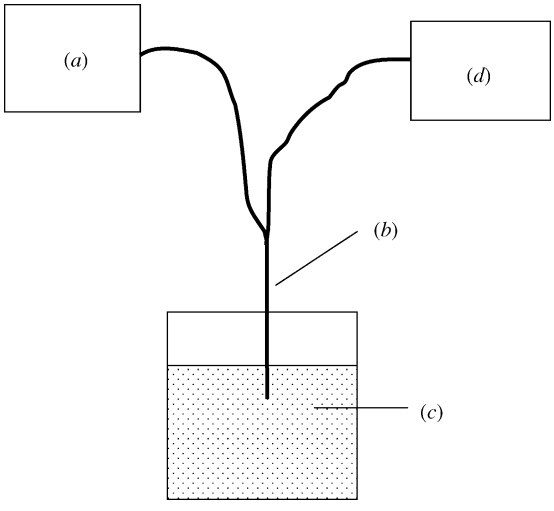

Fig. 1. Scheme of experimental setup. Light source (a); fiber optics bundle (b); electrolyte (c); and photosensor (d).

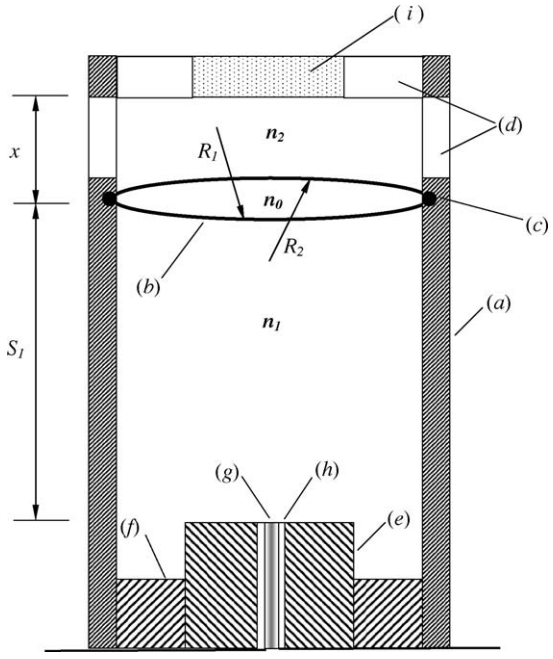

Fig. 2. Sensor scheme. Inner illumination fibers of bundle (g); outer collection fibers of bundle (h); stain less steel jacket (e); PVC holder piece (f); Teflon housing (a); holes for electrolyte (d); lens (b); O-ring seal (c); Teflon screen (i).

One O-ring seal on the lens border (Fig. 2(c)) keeps both parts of the chamber tight, leaving one part immersed in air (air chamber) (Fig. 2(n_1)) and the other one open to be soaked in the electrolyte (electrolyte chamber) (Fig. 2(n_2)) by 10 holes (Fig. 2(d)). The holes are big enough to avoid occasional bubble trapping that can produce incorrect readings. The air chamber (Fig. 2(n_1)) has the tip of the T bundle (Fig. 2(e)) centered by a PVC piece (Fig. 2(f)). The inner and annular fibers of the tip are represented in Fig. 2(g) and (h), respectively. The distance between the bundle tip to the lens is called S_1. The electrolyte chamber (Fig. 2(n_2)) has a Teflon screen in front of the lens (Fig. 2(i)). The distance between the lens and the Teflon screen is called x.

3. Working principle

The sub-bundle corresponding to the inner group of fiber optics is connected to a tungsten lamp and the other one corresponding to the annular group of fibers is connected to the photodiode.

The incoming light emerges from the inner part of the bundle in the air chamber producing an image on the Teflon screen at the electrolyte chamber. The image on the screen is taken as another source of light and comes back through the lens forming a second image on the surface of the bundle tip partially illuminating the annular fibers that collect the light. Small changes in the refraction index of the electrolyte are detected by variations of the ray trajectories modifying the illumination area on the collector fibers over the bundle surface permitting the changes in the electrolyte specific gravity to be detected. In the case of Table 1 [15], the SOC is directly related to the specific gravity of the electrolyte and the SOC. The system can be calibrated by

Table 1
State-of-charge vs. electrolyte density for a SLI battery

State-of-charge	Electrolyte density (g cm^{-3})
100% (full charge)	1.265
75%	1.225
50%	1.190
25%	1.155
Discharged	1.120

simply modifying the distances between bundle-lens (S_1) and lens-screen (x) obtaining a background illumination over the external collector fibers of the bundle.

The design parameters of the optical sensor are the radius of lens and the distances from the bundle to the lens and from the lens to the screen.

4. Optical model and design criteria

Considering the conceptual design of the sensor previously described, it is necessary to solve the problem of the image formation by means of a thin lens in contact with two media of different refraction index at both lens sides as a previous tool for modeling the sensor behavior.

Fig. 3 shows the scheme that we consider for a paraxial ray tracing model of a lens with thickness d and refractive index n_0 in contact with a media of refractive index n_1 (air) on the first interface of curvature R_1, and other media with refractive index n_2 (electrolyte) on the second interface of curvature R_2. In order to calculate the image position that an object placed at the side of n_1 projects on the side n_2, it is necessary to consider the thick lens in two steps. The first one is to calculate the position of the image generated by the first curvature R_1, and the second one is to calculate the final position of the image generated by the second curvature R_2 taking the previous image obtained in step one as the object.

The following expression is used for the first part [16]:

$$\frac{n_1}{S_1} + \frac{n_0}{S^*} = \frac{n_0 - n_1}{R_1} \tag{1}$$

where S^* is the position of the image generated by the first interface or curvature R_1. Taking into account that the position of this image with respect to the second interface of curvature R_2 is $d - S^*$, we can write a similar expression for the second surface:

$$\frac{n_0}{d - S^*} + \frac{n_2}{S_2} = \frac{n_2 - n_0}{R_2} \tag{2}$$

where S_2 is the position of the image in the media of refractive index n_2.

Considering that our lens is a thin lens, thus $d \to 0$, and solving (1) and (2) we can find,

$$\frac{n_1}{S_1} + \frac{n_2}{S_2} = \frac{n_0 - n_1}{R_1} - \frac{n_0 - n_2}{R_2} \tag{3}$$

This expression relates S_1 and S_2 allowing the image position to be calculated. By the way, it is good to see that expression (3) is the well-known Lensmaker's formula [16] for $n_1 = n_2 = 1$ (thin lens full immersed in air).

$$\frac{1}{S_1} + \frac{1}{S_2} = (n_0 - 1)\left(\frac{1}{R_1} - \frac{1}{R_2}\right) \tag{4}$$

The focal distances at both sides of the lens present asymmetric values that are easy to calculate from (3) by doing: $S_1 = \infty$, $S_2 = f_2$ and $S_2 = \infty$, $S_1 = f_1$ (parallel rays coming from the left and right, respectively):

$$f_1 = \frac{n_1}{(n_0 - n_1/R_1) + (n_2 - n_0/R_2)} \tag{5}$$

$$f_2 = \frac{n_2}{n_1} f_1 \tag{6}$$

Note that we are keeping the same nomenclature that is used for the distances inside the chambers of the sensor, and S_2 is not necessarily equal to the distance between the lens and the Teflon screen. Distance S_2 is variable depending on variations of n_2 but the lens-screen distance is a fixed value. Then the image projected on the screen is normally unfocused.

This image is used as a new object for the lens forming back a second image over the fiber optic bundle tip as was explained above. Fig. 4 shows a scheme of a thin lens with asymmetric focal distances as in our case, where the main rays are schematized. The rays that are going from left to right are represented by solid line arrows and the returning rays are represented as dashed line arrows. If we call x the distance from the lens to the Teflon screen in the second chamber, it is easy to find the following

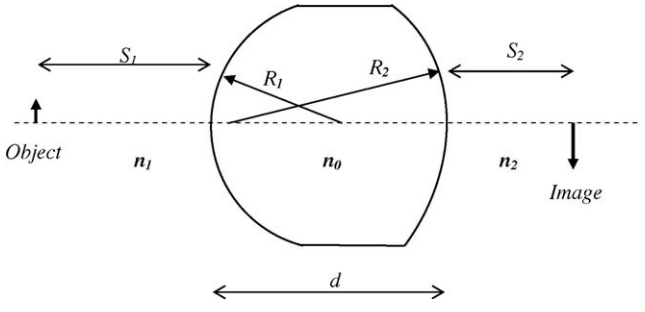

Fig. 3. Lens of thickness d and refractive index n_0 in contact with two different media of refractive indexes n_1 and n_2 at both sides.

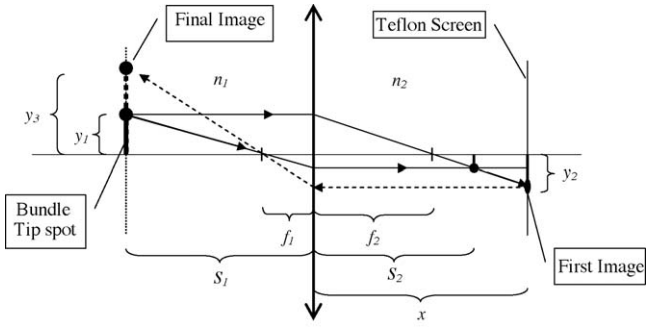

Fig. 4. Elemental ray tracing used for the calculation of the sensor's sensitivity.

relationships from Fig. 4:

$$\frac{y_1}{f_2} = \frac{y_2}{x - f_2} \tag{7}$$

$$\frac{y_2}{f_1} = \frac{y_3}{S_1 - f_1} \tag{8}$$

where y_1, y_2 and y_3 are the spot bundle size, first image size over the Teflon screen and final image size, respectively. By solving (7) and (8) we find the final magnification between the spot bundle size and the final image size:

$$\frac{y_3}{y_1} = \left(\frac{x}{f_2} - 1\right)\left(\frac{S_1}{f_1} - 1\right) = m \tag{9}$$

Finally, if we consider the image shape as a circular spot, the relative increment in the illuminated area over the bundle is:

$$\frac{\Delta A}{A} = m^2 - 1 \tag{10}$$

Assuming a proportional relationship between the relative increments on the illuminated area over the bundle, we can use Eqs. (5)–(10) to design the sensor. Considering the photodiode connected to the annular arrangement of the fiber optics bundle, the output signal must be proportional to $\Delta A/A$.

By using the constructive parameters: R_1, R_2, S_1, x and taking $n_1 = 1.0$ (air), $n_0 = 1.523$ (BK7 glass in the middle of visible spectra), we calculated $\Delta A/A$ for different typical values of n_2.

Fig. 5 shows four different curves of response obtained by solving Eqs. (5)–(10) using a lens of $R_1 = R_2 = 0.5$ cm, and only modifying the values of S_1 and d. The range of change for the refraction index has been estimated according to the Lorentz–Lorenz formula, which connects Maxwell's phenomenological theory with the atomistic theory of matter. By using tabulated data by Born and Wolf [17] for a mixture of water and sulphuric acid, the expected range for the refraction index variation during the cycling process is 1.30–1.38 taking a typical variation of electrolyte density between 1 g cm^{-3} and 1.293 g cm^{-3}.

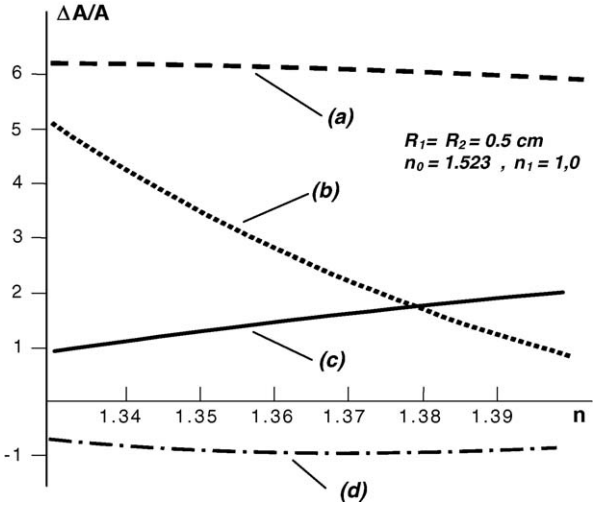

Fig. 5. Behavior for different sets of parameter's sensor: $S_1 = 4$ cm, $x = 0.40$ cm (a); $S_1 = 3.5$ cm, $x = 1.50$ cm (b); $S_1 = 4$ cm, $x = 0.65$ cm (c); and $S_1 = 4$ cm, $x = 1.00$ cm (d).

The curve in Fig. 5(a) shows a flat behavior distinguished by their slopes. Note that small changes in distances produce very different sensor behavior. The curve in Fig. 5(c) presents a positive slope increasing a factor to the illumination area in the expected range. In our case, considering the dimensions of the illumination fibers (center of bundle) and receptive fibers (annular arrangement), the curve in Fig. 5(c) fits the aspect ratio of the bundle utilized very well. In contrast, the curve in Fig. 5(b) is not a good choice for our system because for variations higher than 2.5 in the illuminated area, the light drops out of the annular arrangement and the sensor does not work properly. However, that choice may be made suitable by using a bundle selected with the adequate aspect ratio between inner and annular fibers. The curve in Fig. 5(d) is a solution with a negative value of $\Delta A/A$ determined by a virtual image.

On the other hand, checking a similar optical sensor but with both sides of the lens embedded in the electrolyte, i.e., in our case considering both chambers open to be fulfilled by the electrolyte the behavior is similar to that previously described except for an increase of about 3 cm in S_1. By increasing the diffraction index inside the first chamber to the same value of BK7 glass, i.e., considering a thick lens fulfilling the entire volume of the first chamber, S_1 increases more than 10 cm. In this work, we prefer to use the optical sensor designed to keep the minimum dimensions, taking into account the usual lack of available space inside a battery cell. This is the reason why the arrangement with the first chamber embedded in air has been chosen. Note that the election of an adequate set of parameters is critical in order to obtain a linear response as well as high sensitivity.

5. Experimental results

An SLI lead-acid battery of 12 V, 45 A h was cycled by using an Einhell AFN9 bipolar power supply during a 19 h test that included a 2 h rest between the discharge and charge processes.

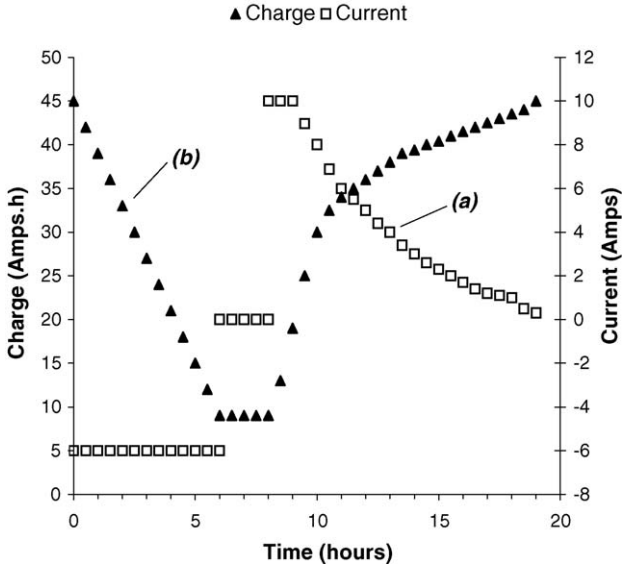

Fig. 6. Current (a) and state-of-charge (b) vs. time during the cycling test of battery.

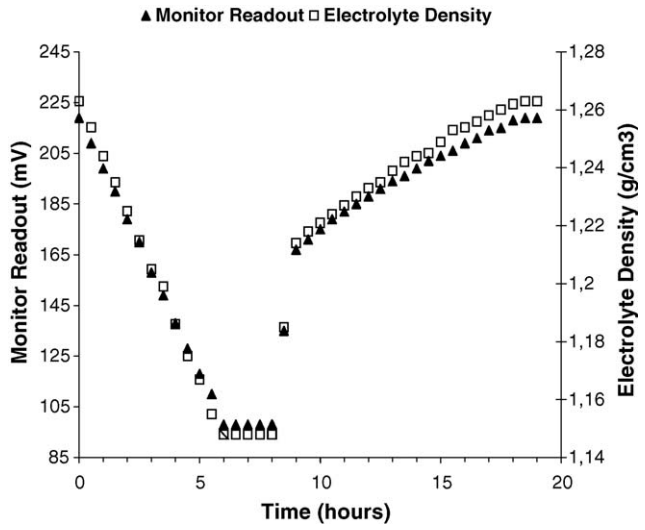

Fig. 7. Monitor readout and electrolyte density vs. time during cycling test of battery.

Current evolution was recorded and the electrolyte density was determined by weighing samples of 50 cm^3 every 30 min.

Fig. 6 shows the current and charge curves of the cycling process applied to the battery. These curves show a first stage in which the battery was discharged at 6 A for 6 h, following a 2 h rest period. The final SOC after the first stage was estimated in 9 A h in agreement with an electrolyte density measurement of 1.148 g cm^{-3} corresponding to 20% of the full charge [13]. A last stage of charging for 11 h was performed after the rest period. Notice that the current limitation of 10 A exists in order to avoid the temperature increase for the mildly exothermic charging reaction in this kind of battery. The curve of charge in Fig. 6(b) was calculated by integration of current.

Fig. 7 shows the curves of electrolyte density and monitor readout versus time where the agreement between both measurements is remarkable. Fig. 8 shows the state-of-charge estimated by integration of current and the monitor readout versus time. It exhibits excellent agreement between both measurements with deviations lower than 4%.

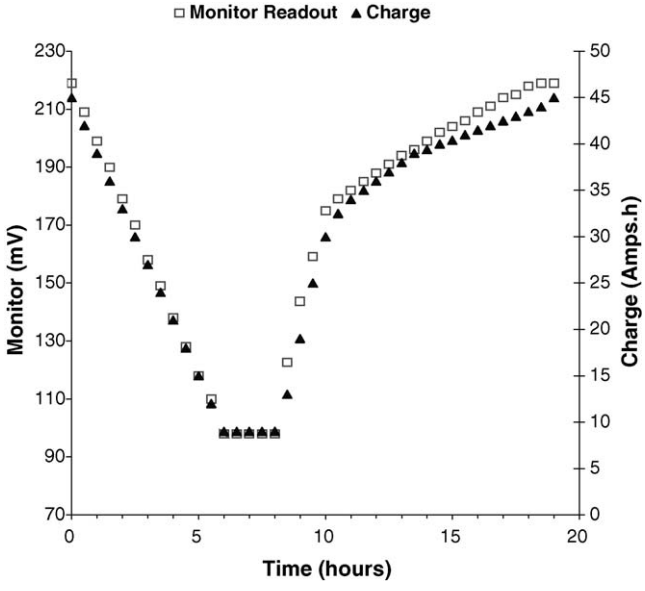

Fig. 8. Monitor readout and state-of-charge vs. time during cycling test of battery.

6. Conclusions

A fiber optic system for measuring relative density of the electrolyte in a lead-acid battery has been developed and applied successfully to the state-of-charge measurement. The method is based on measuring the variation of light ray deflection produced in the electrolyte media when its density changes. A simple lens is used in order to magnify the changes detected by a photodiode. Electronic amplification or any other signal processing is not necessary. The linearity and range behavior of the sensor can be predicted by using an analytical ray tracing set of equations. Important changes associated with small variations in the constructive parameters are observed experimentally and are also predicted theoretically. Therefore, the alignment of components inside the sensor is a critical issue. The instrument can be used for remote monitoring of the SOC of lead-acid batteries, exhibiting real advantages with respect to previous research, based on its high level of simplicity, robustness and low cost. According to the results obtained placing the sensor at different heights inside each cell, the variations in the electrolyte density from the bottom to the top of cell can produce an influence lower than 2%. This good behavior is due to the low rate of charge used during the experiments (slow charge), for faster charging rates the sensor presents a serious limitation giving a typical deviation of 15%. Another limitation of the system is the response time due to the slow electrolyte diffusion velocity to and from the sensor cavity. Such problem is negligible while the rate of charge is lower than 10 A, but must be taken into account for fast charging rates. The increasing electrolyte turbidity with the time due to particles coming from the plates may be other source of bad readouts. This effect and the ageing of the light source can be solved by means of a reference cell included in the system in order to perform an automatic calibration to correct possible drifts in the measurements. Temperature correction by using a simple thermocouple embedded in the electrolyte is also recommended for final applications. Finally, the dimensions of the sensor can be drastically reduced by using a smaller bundle and optics. This possibility can be exploited for practically all type of acid batteries including the cells of VRLA batteries where the lack of space is an important problem for this kind of invasive sensors.

References

[1] D.C. Cox, R. Prez-Kite, 22nd International Telecommunications Energy Conference, INTELEC. Phoenix, AZ, USA, 2000, p. 342.
[2] S. Wakida, S. Mochizuki, R. Makabe, A. Kawahara, M. Yamane, S. Takasuka, K. Higashi, International Conference On Solid State Sensors and Actuators, Digest of Technical Papers, San Francisco, CA, USA, 1991, p. 222.
[3] C.S.C. Bose, F. Laman, 22nd International Telecommunications Energy Conference, INTELEC. Phoenix, AZ, USA, 2000, p. 597.

[4] I. Buchamann, 16th Annual Battery Conference on Applications and Advances, Long Beach, CA, USA, 2001, p. 263.
[5] I.R. Hill, E.E. Andrukaitis, J. Power Sources 103 (2001) 98.
[6] P.R. Stevenson, US Patent No. 5,093,624 (1992).
[7] D. Limuti, J.M. Ross, T.L. Churchill, US Patent No. 5,132,626 (1992).
[8] J.F. Beutler, B.J. Burreson, W.A. van Schalkwijk, D.F. Flagg, G.A. Kromholtz, J.J. Green, US Patent No. 5,537,042 (1996).
[9] F.C. Peterson, US Patent No. 4,308,817 (1982).
[10] J.L. Hinkle, US Patent No. 4,866,428 (1989).
[11] J.D. Weiss, US Patent No. 5,949,219 (1999).
[12] G.P. Hancke, Proceedings of the IEEE Instrumentation and Measurement Technology Conference, Washington DC, USA, 1989, p. 486.
[13] www.oceanoptics.com.
[14] www.thorlabs.com.
[15] D. Linden, T.B. Reddy (Eds.), Handbook of Batteries, McGraw-Hill, New York, 2002 (Chapter 23).
[16] E. Hecht, Optics, Adisson Wesley Longman Inc., New York, 1998 (Chapter 5).
[17] M. Born, E. Wolf, Principles of Optics, Cambridge University Press, London, 1999 (Chapter 2).